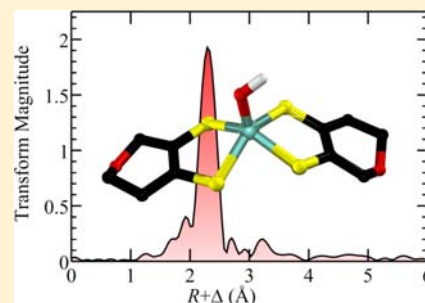


X-ray Absorption Spectroscopy of a Quantitatively Mo(V) Dimethyl Sulfoxide Reductase Species

M. Jake Pushie,[†] Julien J. H. Cotelesage,^{†,‡} Ganna Lyashenko,[§] Russ Hille,[§] and Graham N. George^{*,†}[†]Molecular and Environmental Sciences Research Group, Department of Geological Sciences, University of Saskatchewan, SK, S7N 5E2, Canada[‡]Canadian Light Source, 101 Perimeter Road, Saskatoon, SK, S7N 0X4, Canada[§]Department of Biochemistry, University of California-Riverside, Riverside, California 92521, United States

ABSTRACT: Molybdenum K-edge X-ray absorption spectroscopy (XAS) has been used to probe the structure of a Mo(V) species that has been suggested to be a catalytic intermediate in the reaction of dimethyl sulfoxide (DMSO) reductase with the alternative substrate trimethylamine N-oxide (Bennet et al. *Eur. J. Biochem.* **1994**, *255*, 321–331; Cobb et al. *J. Biol. Chem.* **2005**, *280*, 11007–11017; Mtei, et al. *J. Am. Chem. Soc.* **2011**, *133*, 9672–9774). The oxidized Mo(VI) state of DMSO reductase has previously been structurally characterized as being six coordinate, with four sulfurs from pyranopterin dithiolene molybdenum cofactors, a terminal oxygen ligand, and an additional oxygen coordination from a serine residue. We find the most plausible structure for the Mo(V) active site is a five-coordinate species with four sulfur donors from the two pyranopterin dithiolene ligands, with an average Mo–S bond-length of 2.35 Å, plus a single oxygen donor at 1.99 Å, very likely from an Mo–OH ligand. Our results thus suggest that the oxygen of the serine residue has dissociated from the metal ion, suggesting hitherto unsuspected flexibility of the active site, and calling into question whether this putative intermediate is catalytically relevant. The relevance to previous Mo(V) electron paramagnetic resonance and other spectroscopic studies on DMSO reductase is discussed. XAS of an extensively studied Mo(V) form of *Rhodobacter sphaeroides* DMSO reductase (the high-g split species) shows that previously suggested structures for the active site are likely incorrect.



■ INTRODUCTION

Molybdenum and tungsten are respectively the only second and third transition elements that have confirmed roles in biology.^{1,2} The molybdenum and tungsten enzymes form a distinctive group which possesses either one or two pyranopterin cofactors coordinated to the metal through an enedithiolate group (Figure 1), with the tungsten enzymes probably representing evolutionarily more ancient forms than the molybdenum enzymes.³ The enzyme nitrogenase contains molybdenum or vanadium within a novel iron–sulfur cluster, and is considered to be quite distinct from these enzymes. Nitrogenase is therefore placed in a unique category of its own, and is not relevant to the work presented here. The molybdenum and tungsten enzymes fulfill diverse physiological functions, playing vital roles in the global nitrogen and carbon cycles and in the microbial detoxification of species such as arsenite, selenite, and chlorate.^{1,2} In almost all cases the enzymes catalyze reactions that involve two-electron oxidation–reduction chemistry coupled to the transfer of an oxygen atom to, or from, water. The *Rhodobacter* dimethylsulfoxide (DMSO) reductases are among the best studied of the molybdenum enzymes,⁴ and are considered to be the prototypical member of the DMSO reductase family of Mo enzymes. DMSO reductase from photosynthetic bacteria such as *Rhodobacter sphaeroides* and *Rhodobacter capsulatus* catalyzes

the final step in the respiratory chain when the organisms are using DMSO as the terminal electron acceptor:



The enzyme is capable of interacting with a range of substrates and products,^{5,6} including trimethylamine N-oxide [(CH₃)₃NO],^{6,7} and is unusual among the molybdenum enzymes in having only the molybdenum site as a prosthetic group, with no iron–sulfur clusters or other cofactors bound. The active site of the oxidized Mo(VI) enzyme is six coordinate with two pyranopterin dithiolene ligands providing four sulfur donors to the metal, one terminal oxygen ligand and a coordinated serine residue.^{8–11} Mo(V) electron paramagnetic resonance (EPR) spectroscopy has been extensively used to study the active sites of molybdenum enzymes, and a number of different studies have examined the Mo(V) EPR of *Rhodobacter* DMSO reductases.^{4,7,9,12} In general, the most readily obtained EPR signal is that termed high-g split by Bennett et al.¹² which has been suggested to have catalytic relevance.^{6,7,9} The signal is insensitive to pH, but does show slight sensitivity to buffer conditions and the specific manner in which it is generated.^{9,12} It has rhombic g-values with $g_{x,y,z}$ values close to 1.99, 1.98, and 1.97, and shows slightly

Received: July 28, 2012

Published: February 27, 2013

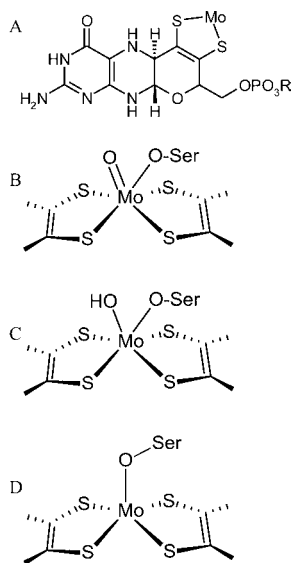


Figure 1. (A) Structure of the molybdopterin cofactor, the group *R* can be H, guanosine, or cytosine, depending on the enzyme (DMSO reductase contains guanosine). (B) The structure derived from crystallography and EXAFS of the oxidized Mo(VI) active site. (C) The structure postulated for the Mo(V) high-*g* split signal giving species. (D) The structure postulated for the fully reduced Mo(IV) species.

anisotropic hyperfine coupling to a single exchangeable proton with $A_{x,y,z}$ values close to 30 MHz.¹² When generated in $H_2^{17}O$ enriched water, the high-*g* split signal also shows anisotropic hyperfine coupling to one exchangeable oxygen,⁹ and both the coupled exchangeable proton and oxygen are thought to originate from an Mo–OH group.^{4,9} Reductive and oxidative titrations in the absence of substrate or product indicate midpoint potentials of +37 mV and +83 mV for the Mo(IV)/Mo(V) and Mo(V)/Mo(VI) couples, respectively.⁹ This species has been studied by a combination of EPR and magnetic circular dichroism (MCD) spectroscopies, together with density functional theory (DFT) calculations, the results being interpreted in the context of an $L_2Mo^V(OH)(O-Ser)$ structure for the signal-giving species, with *L* being the bidentate enedithiolate of the pyranopterin.⁷ The high-*g* split signal can be generated by adding a variety of exogenous reductants to DMSO reductase,¹² is not associated with bound substrate or product, and is quite distinct from Mo(V) EPR signals that do arise from product complexes.¹³

X-ray absorption spectroscopy (XAS) has been essential in developing our understanding of the active site structures of molybdenum enzymes,⁴ but information from XAS on the Mo(V) oxidation states complementary to that from Mo(V) EPR is generally hard to obtain. This is because XAS inevitably detects all of the molybdenum present, and many Mo(V) EPR signal-giving species only accumulate to 10–20% of the total Mo.⁴ Previous XAS studies on DMSO reductase Mo(V) species have thus been limited to the glycerol-inhibited form which shows close to 100% Mo(V), and has a substantially modified metal coordination in which a vicinal diol is bound to Mo.⁸ The recent finding of an essentially quantitatively Mo(V) DMSO reductase trimethylamine N-oxide Mo(V) species from active enzyme⁶ thus provides a novel opportunity to study the structure of a Mo(V) species. Moreover, the Mo(V) signal that this species shows is the well-known high-*g* split signal,^{6,7} so that direct structural information on this species has relevance

to a significant body of prior work. We report herein a study of the Mo(V) DMSO reductase trimethylamine N-oxide species using XAS.

MATERIALS AND METHODS

Samples. DMSO reductase in the Mo(V) trimethylamine N-oxide treated form was prepared as previously described.⁷ XAS samples were prepared by first reducing the enzyme (in 50 mM KH_2PO_4 , 0.6 mM EDTA, pH 6.0) with sodium dithionite, followed by reoxidation with excess DMSO (so-called “redox-cycling”⁹), followed by size exclusion chromatography to remove excess reagents. The enzyme was then concentrated to approximately 5 mM using an Amicon 50 kDa cutoff filter. Oxidized enzyme was used as such for the preparation of a sample of oxidized enzyme, being loaded into ($2 \times 10 \times 10$ mm) acrylic cuvettes and frozen on liquid nitrogen. For fully reduced enzyme, the sample was placed in a glovebox, made 140 μ M in methylviologen and reduced by addition of aliquots of a concentrated solution of sodium dithionite prior to loading into the cell and freezing in dry ice/acetone prior to removal from the glovebox. For the Mo(V) sample, enzyme was further concentrated to ~ 7 mM. A 160 μ L portion of enzyme solution was then mixed with 60 μ L of 150 mM TMAO and 150 μ L of ~ 150 mM sodium dithionite to give the following respective concentrations for Mo, TMAO, and dithionite: ~ 3 mM, 24 mM, 61 mM. Parallel samples, one for XAS and one for EPR, were frozen after 60 s of reaction (during which time the sample was loaded into the acrylic cell). Formation of the “high-*g* split” signal, devoid of other EPR-active species, was confirmed by EPR as previously demonstrated.⁶

XAS Data Collection. XAS measurements were conducted at the Stanford Synchrotron Radiation Laboratory with the SPEAR storage ring containing close to 350 mA at 3.0 GeV, using the data acquisition program XAS Collect.¹⁴ Molybdenum K-edge data were collected on the structural molecular biology XAS beamline 7–3, and employing a Si(220) double-crystal monochromator. Beamline 7–3 is equipped with a rhodium-coated vertical collimating mirror upstream of the monochromator, and harmonic rejection was accomplished by setting the mirror cutoff angle to 23 keV. Incident and transmitted X-ray intensities were monitored using nitrogen-filled ionization chambers using a sweeping voltage of 1.6 kV, and X-ray absorption was measured as the Mo K_{α} fluorescence excitation spectrum using an array of 30 germanium detectors.¹⁵ During data collection, samples were maintained at a temperature of approximately 10 K using an Oxford instruments liquid helium flow cryostat. For each data set, eight scans each of 35 min duration were accumulated, and the energy was calibrated by reference to the absorption of a molybdenum foil measured simultaneously with each scan, assuming a lowest energy inflection point of 20003.9 eV. The energy threshold of the extended X-ray absorption fine structure (EXAFS) oscillations ($k = 0 \text{ \AA}^{-1}$) was assumed to be 20025.0 eV.

XAS Data Analysis. The EXAFS oscillations $\chi(k)$ were quantitatively analyzed by curve-fitting using the EXAFSPAK suite of computer programs¹⁶ as described by George et al.,¹⁷ using ab initio theoretical phase and amplitude functions calculated using the program FEFF version 8.25.^{18,19} No smoothing, filtering, or related operations were performed on the data.

In EXAFS curve-fitting analyses improvements in the fit-error function F are sometimes obscured by the contribution to the error function arising from high-frequency noise in the experimental EXAFS data. In the present work we use the so-called normalized F -value $F = (\sum k^6 (\chi(k)_{\text{calc}} - \chi(k)_{\text{expt}})^2 / \sum k^6 \chi(k)_{\text{expt}}^2)^{1/2}$, with the summation being over data points included in the fit. The contribution of high-frequency noise F_0 to the fit-error function F can be effectively estimated by computing F for the back-transform of the product of a half-Gaussian window function placed above the highest bond-length considered in the fit and the complex discrete Fourier transform, which will extend to $R_{\text{max}} = 2\pi/\delta k$, where δk is the k -space point separation. Thus, for the data analyzed herein, we used a window position of 4.5 \AA (width 0.3 \AA) to estimate an F_0 value of 0.1338, and this can be subtracted from F

to yield $(F - F_0)$ which better illustrates the relative difference between the fits of different models.

Density Functional Theory. DFT calculations employed Dmol³ Materials Studio Version 5.5,^{20,21} using the Perdew–Burke–Ernzerhof functional^{22,23} for both the potential during the self-consistent field procedure and the energy. Dmol³ double numerical basis sets included polarization functions for all atoms, were spin-unrestricted, and all electron relativistic core treatments were used. Solvation effects were modeled by using the Conductor-like Screening Model (COSMO)²⁴ with the dielectric constant of water ($\epsilon = 78.39$). We note that while this is a reasonable value for solvent-accessible sites such as that of DMSO reductase we find that the use of a lower value, more typical of hydrophobic environments, (e.g., $\epsilon = 4$ or 5) affects bond-lengths to Mo by less than 0.005 Å (not illustrated).

RESULTS AND DISCUSSION

XAS. Figure 2 shows the Mo K-edge EXAFS oscillations and corresponding Fourier transform, together with the results of

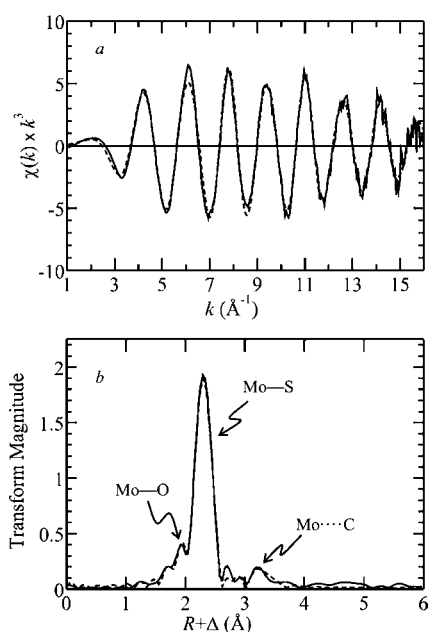


Figure 2. Mo K-edge EXAFS data (a) and corresponding Mo–S phase-corrected EXAFS Fourier transform (b) (solid lines) plus best fits (dashes lines) corresponding to Table 1D.

curve-fitting analyses, which are summarized in Table 1. As expected, the data are dominated by the intense backscattering from four Mo–S interactions arising from the two dithiolene ligands to the metal, and these are responsible for the intense Fourier transform peak at approximately 2.3 Å. Also as expected, the lack of a distinctive Fourier transform peak at about 1.7 Å unambiguously indicates that the active site is *des-oxo*. Longer Mo–O features are typically seen in the Fourier transform as peaks at about 1.9 Å or within the intense Mo–S envelope, although EXAFS curve-fitting analysis is typically required to deconvolute these components. The EXAFS Fourier transform also shows a small but well-defined peak at about 3.4 Å, which is often seen in spectra of molybdenum enzymes, and arises from Mo...C backscattering from the dithiolene carbon ligands.

The commonly accepted structure for the high-*g* split Mo(V) form of the enzyme is six-coordinate^{7,9} and analogous to the oxidized Mo(VI) form studied using crystallography and EXAFS (Figure 1 B), but with the Mo=O group gaining a

proton to form Mo–OH (Figure 1 C); the proton of the Mo–OH group is thought to give rise to the proton hyperfine splitting observed by EPR.^{4,7,9} The alternative structures that we will consider for the Mo(V) high-*g* split EPR signal-giving species are shown schematically in Figure 3. The EXAFS curve-fitting analysis clearly shows metal coordination to four sulfurs with Mo–S bond lengths of 2.35 Å, but is not obviously consistent with coordination by two oxygen ligands (Table 1). Determination of accurate coordination numbers using EXAFS can be problematic, so that some caution is justified in the interpretation of the data. The primary reason for uncertainty is that the Debye–Waller factor $e^{-2\sigma^2 k^2}$ (where k is the photoelectron wave-vector and σ^2 the mean-square deviation in bond-length R) and the coordination number N show a high degree of mutual correlation in the refinement of structural models to the data. The value of σ^2 has components corresponding to vibrational and static variance in R , such that $\sigma^2 = \sigma_{\text{vib}}^2 + \sigma_{\text{stat}}^2$ for homogeneous samples and $N = 1 + \sigma_{\text{stat}}^2$ is zero, and when $N > 1$ an upper bound for σ_{stat}^2 can be estimated from the k -range of the data.⁹ We have previously discussed methods for calculation of σ_{vib}^2 ^{9,25,26} and for Mo–O groups with bond-lengths close to 2 Å we expect σ^2 values in the range of 0.0027–0.0036 Å². For the present data, inclusion of only a single Mo–O clearly gives the most satisfactory fit, albeit with a somewhat larger than expected σ^2 value, and constraining the latter to the minimum value expected gives a slightly worse fit. If two Mo–O groups are forced to be present in the refinements the σ^2 value of one Mo–O increases to a chemically unreasonable value that is sufficient to reduce the contribution to only 1.1% of the total EXAFS amplitude, effectively removing the contribution of this oxygen to the total EXAFS (Table 1F). Fitting the data with two Mo–O distances and constraining the individual σ^2 values to chemically reasonable limits gives a significantly poorer fit. Figure 4 shows search profiles for an Mo–O interaction in which the fit error is plotted as a function of bond-length R vs coordination number N and N vs σ^2 , illustrating well-defined minima corresponding to $R = 1.99$ Å, $N = 1.0$, and $\sigma^2 = 0.0051$ Å². We note that the presence of a very large σ_{stat}^2 possibly for the Mo–OH ligand, which might be due to a large number of available structural conformations of this group within the active site, could potentially hide an additional oxygen backscatterer. However, such a phenomenon would be expected to give rise to significant *g*-strain which is inconsistent with the observed narrow Mo(V) EPR linewidths of the high-*g* split signal. Moreover, DFT calculations of the energy variation on moving the Mo–OH group indicates quite a sharp minimum (not illustrated), and we therefore do not consider this possibility likely. The species studied here thus appears structurally quite distinct from the six-coordinate Mo(IV) product complexes that we have previously studied,⁵ as illustrated by a comparison of the EXAFS Fourier transforms in Figure 5 which can be seen to be quite distinct. The EXAFS portion of the XAS spectrum is not directly sensitive to oxidation state, and bond-lengths for Mo(V) and Mo(IV) species will be very similar (iso-structural Mo(V) species should have slightly shorter bond-lengths relative to Mo(IV) by ~ 0.01 Å),^{4,27} so that the differences shown in Figure 5 are largely due to the active site having different structures in the two species.

There is also a possibility that EXAFS cancellation effects may be present in the data. These occur when the EXAFS from two different backscatterers are coincidentally of opposite

Table 1. Selected EXAFS Curve Fitting Results^a

fit	Mo–S			Mo–O			Mo···C			ΔE_0	F	$(F-F_0)$
	N	R	σ^2	N	R	σ^2	N	R	σ^2			
A	4	2.353(1)	0.0036(1)							–17.1 ^b	0.2247	0.0909
B	4	2.353(1)	0.0035(1)	1	1.989(6)	0.0051(5)				–17.1 ^b	0.1919	0.0581
C	4	2.355(1)	0.0035(1)	2	1.992(8)	0.0114(11)				–17.1 ^b	0.2174	0.0836
D	4	2.354(1)	0.0035(1)	1	1.990(5)	0.0051(5)	4	3.394(6)	0.0049(6)	–17.1(3)	0.1749	0.0411
E	4	2.353(1)	0.0031(1)	1	2.000(6)	0.0057(6)	4	3.394(6)	0.0042(6)	–17.1(3)	0.1759	0.0421
				1	2.357 ^c	0.0037 ^c						
F	4	2.355(1)	0.0034(1)	1	1.990(8)	0.0046(4)	4	3.398(7)	0.0050(6)	–17.0(3)	0.1759	0.0421
				1	2.24(3)	0.012(10)						
G	4	2.355(1)	0.0034(1)	1	1.958(6)	0.0027 ^d	4	3.394(6)	0.0049(6)	–17.2(3)	0.1933	0.0595
				1	2.092(8)	0.0029 ^d						
H	4	2.355(1)	0.0034(1)	1	1.987(2)	0.0027 ^d	4	3.395(6)	0.0049(6)	–17.3(3)	0.1857	0.0519

^aCoordination numbers, N , interatomic distances R (Å), Debye–Waller factors σ^2 (Å²), and threshold energy shift ΔE_0 (eV). The fit error parameters F and $(F - F_0)$ are described in the Materials and Methods section. Values shown in bold represent the best fit obtained. Values in parentheses are the estimated standard deviations obtained from the diagonal elements of the covariance matrix; these are precisions and are distinct from the accuracies which are expected to be larger (ca ± 0.02 Å for R , and $\pm 20\%$ for N and σ^2), and that relative accuracies (e.g., comparing two different Mo–S bond-lengths) will be more similar to the precisions. The amplitude scale factor, otherwise known as the many-body amplitude reduction factor, or S_0^2 , was defined by fitting data from a number of model compound species as 1.05. In all cases the k -range of the data fitted was from 1.0 to 16.2 Å^{–1}. ^bThis parameter was constrained to a value determined by fitting model compounds. ^cParameters constrained to values that are most effectively canceled by the Mo–S interaction. ^dThis parameter was constrained to a chemically reasonable value.

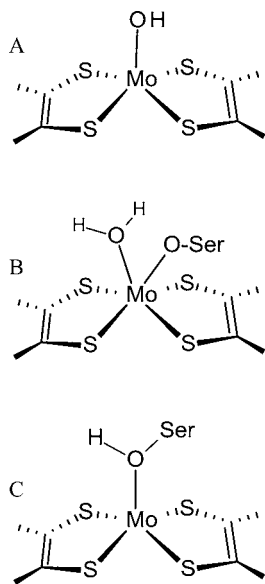


Figure 3. Alternative structures for the Mo(V) high-g split EPR signal-giving species.

phase, so that the contribution from one can be hidden by cancellation with all or part of the other. This possibility has been discussed previously both in general^{26–29} and specifically for the molybdenum enzymes.³⁰ The predominant EXAFS in our case arises from the 2.35 Å Mo–S interaction (Table 1), and the EXAFS phase functions for Mo–O and Mo–S within the k -range of our data are inherently almost 180° out of phase so that an Mo–O bond at this same length should be very hard to detect. Thus, we calculate that an Mo–O bond at 2.36 Å will provide effective cancellation with the 2.35 Å Mo–S, resulting in a decrease in sulfur amplitude by corresponding to $N \approx 0.5$ or with a slightly decreased σ^2 value, plus a slight amplitude miss-match at both high and low k ends of the data. EXAFS refinements constrained to this cancellation condition converged on a solution with a slightly decreased Mo–S σ^2 value, with a fit error only slightly worse than the best fit (Table 1).

This bond-length is consistent with coordinated water, and this is confirmed by a search of the Cambridge Structural database²⁷ for sulfur-coordinated molybdenum species with Mo–O bonds close to 2.36 Å, excluding structures with groups eliciting *trans* effects such as Mo=O groups, which yields only Mo–OH₂ species. Our data are thus consistent with either a five coordinate structure with a single Mo–O group (Figure 3 A) or a six coordinate structure where one of two oxygen ligands is from coordinated water (Figure 3 B). Mo(V) coordinated water would be expected to give two strongly coupled exchangeable protons in the Mo(V) EPR signal, which is not observed. Although it is possible that one of the two protons might have a hyperfine too weak to be detected by conventional means, we consider this possibility less likely than a five coordinate site. A search of the Cambridge Structural database²⁷ for Mo(V) species with coordination environments resembling those of Figure 3 A or B yields no results at all, but there are a number of examples of analogous coordination environments for Mo(IV) species.^{33,34} For six-coordinate species with two Mo–O groups, average Mo–O bond-lengths close to 2.19 Å are observed, and average Mo–S bond-lengths of 2.32 Å. For five-coordinate species an average bond-lengths of 1.86 Å and 2.33 Å are expected for Mo–O and Mo–S, respectively.²⁷ The bond-lengths for iso-structural Mo(V) and Mo(IV) species will be similar, with slightly shorter bond-lengths for Mo(V) by approximately 0.01 Å.^{4,27} The Mo–S bond-lengths determined for our Mo(V) DMSO reductase species agree reasonably well with values from these complexes, but the single Mo–O at 1.99 Å is significantly longer than the average bond-length of the model species at 1.86 Å, and slightly longer than the longest of these at 1.93 Å,³⁴ and this raises the possibility of a protonated serine coordination as shown in Figure 3 C. The Cambridge Structural Database reveals a number of structurally characterized Mo–OH–CH₂ with a number of these being Mo(V) species, which show Mo–O bond-lengths in the range 2.08 to 2.26 Å.²⁷

Overall, the available data lead to the unexpected conclusion that there is probably only a single Mo–O ligand in the high-g

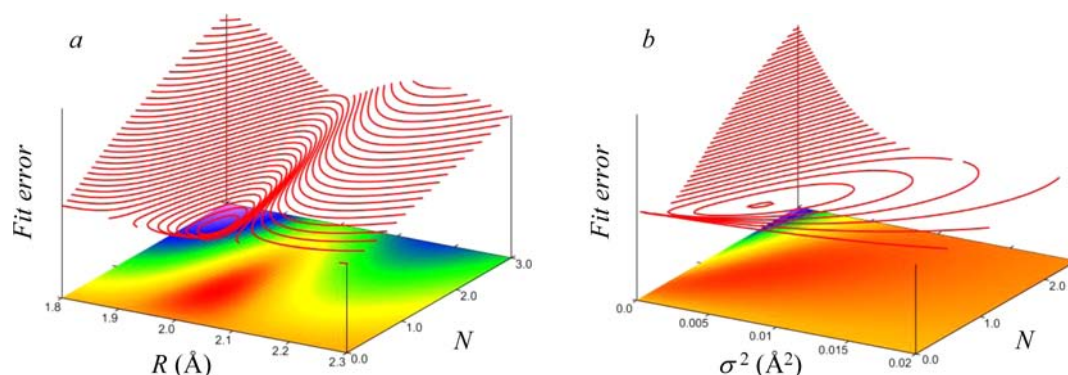


Figure 4. EXAFS curve-fitting search profiles of (a) bond-length R versus coordination number N and of (b) the mean-square deviation in bond-length σ^2 versus N , showing the minimum in fit error at $R = 1.99$ Å and $N = 1.0$ for Mo–O. Note that the range for N in (b) has been reduced slightly to adequately show the minimum at $\sigma^2 \sim 0.005$ Å² and $N \sim 1$.

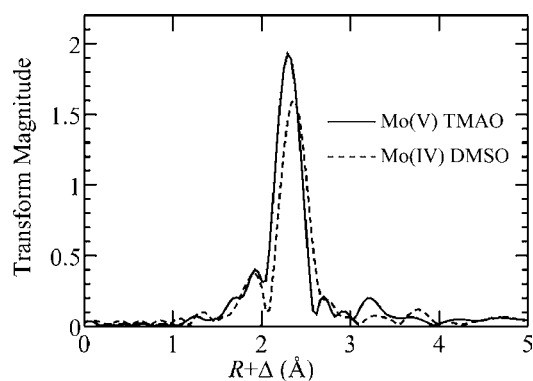


Figure 5. Comparison of the EXAFS Fourier transforms (phase-corrected for Mo–S) for the DMSO reductase six-coordinate Mo(IV) DMSO-bound species, and the Mo(V) trimethylamine N-oxide species.

split Mo(V) species of DMSO reductase. The observed hyperfine coupling to a single exchangeable proton in the Mo(V) EPR spectrum indicates that either an Mo–OH or Mo–(OH)–C group is present in the signal giving species (Figure 3), and the curve-fitting analysis supports as either structures for the Mo(V) EPR signal-giving species as possible Figure 3 A or C with four Mo–S bonds and a single Mo–O. Insofar as choosing between these two models is concerned previous Mo(V) EPR of the high- g split species developed in isotopically enriched water (H_2^{17}O) conclusively shows the presence of a single exchangeable oxygen in the signal giving species.⁹ The oxygen of the protonated serine of Figure 3C would not be expected to be exchangeable, whereas that of Figure 3A should readily exchange with solvent water. We therefore conclude that all of the available data on the high- g split signal giving species support only the structure of Figure 3A.

The suggestion that a serine oxygen ligand to Mo might dissociate is ostensibly a somewhat novel suggestion, but not without some precedent in DMSO reductase and among the molybdenum enzymes more generally. It has previously been reported that recombinant *R. sphaeroides* DMSO reductase from *E. coli* can be isolated in a vivid green form that has a *cis*-dioxo Mo with four nearly equivalent sulfur donors from the two cofactor dithiolenes and no other ligands (i.e., without oxygen coordination from Ser147). This form lacks Mo^V EPR spectra, and the normal oxidized enzyme with a coordinated Ser147 can be regenerated by a cycle of reduction and

oxidation.⁹ The glycerol-inhibited form of the enzyme^{8,12,36} can also be made nearly quantitatively Mo(V), but with quite different Mo(V) EPR spectra from that of high- g split species, most notably lacking hyperfine splitting from a solvent exchangeable proton.^{7–9,36} Our previous EXAFS analysis indicates that the glycerol-inhibited form of the enzyme is six-coordinate with four Mo–S ligands and two from Mo–O. The lack of proton hyperfine splitting, along with the fact that monoalcohols do not form related inhibited species, has been taken to indicate that this species has Ser147 dissociated with the vicinal diol of the glycerol (or ethylene glycol) providing the two oxygen ligands to Mo.⁸ This species has very similar MCD to the high- g split species, despite different Mo(V) EPR and XAS, and this may be attributed to the fact that transitions arising from the dithiolene π -system dominate the MCD.^{7,36,37} Thus, the effects of the protein in constraining molybdopterin orientation in DMSO reductase may mean that the active site is sufficiently constrained that a change from 6- to 5-coordination may not require any large change in geometry of the dithiolenes and Mo. This in turn might make differences in the MCD rather subtle. Reduction of oxidized DMSO reductase with triphenylphosphine yields a yellow mono-oxo species with four sulfur ligands that also appears to lack coordination by Ser147.⁵ Redox-dependent dissociation of a serine side-chain ligand to molybdenum has also previously been observed in the cysteine 207 \rightarrow serine mutant of human sulfite oxidase.³¹ In the oxidized form of the enzyme the coordination is modified from the wild-type; a *cis*-dioxo molybdenum with three sulfur ligands (two from a single pyranopterine dithiolene and one from cysteine 207), to a *cis*-trioxo molybdenum with two sulfurs and lacking coordination by serine 207.^{17,31,32} In the course of reductive titrations, serine 207 coordinates to the molybdenum in both Mo(V) and Mo(IV) and dissociates again on subsequent reoxidation to Mo(VI).³¹ In other molybdenum enzymes differential coordination of an amino acid side chain has also been observed. For the respiratory nitrate reductase from *Escherichia coli* Bertero et al. have used crystallography to suggest a bidentate coordination of aspartate 222 to a des-oxo Mo site,³⁵ while Jormakka et al. obtain a monodentate aspartate 222 coordination to a mono-oxo Mo site.³⁸ The fact that the dithiolene ligands to Mo from the cofactor can dissociate in DMSO reductase^{4,11,39} and related enzymes^{4,40} is now well established, and atmospheric oxygen and certain buffers appear to be co-conspirators in causing this.³⁹ Collectively these observations illustrate that the active sites of Mo enzymes in general, and of DMSO reductase in particular, exhibit

significant malleability and establish precedent for our suggestion that Ser147 can dissociate from Mo.

In DMSO reductase the formation of the Mo(V) high-*g* split species is not accompanied by any permanent loss of activity, and so if serine dissociation occurs it must be reversible. Most previous work on DMSO reductase has assumed that the oxygen ligand from serine 147 is a relatively invariant active site component. Webster and Hall⁴¹ have used DFT calculations to suggest that in the DMSO complex with the enzyme in the Mo(IV) state, partial bond formation between the sulfur of DMSO and oxygen of Serine 147 with a S...O bond of about 2.45 Å stabilizes the binding of DMSO, although formation of a similar complex with sterically more crowded trimethylarsine oxide argues against this.⁵ Modification of serine 147 to a cysteine changes the molybdenum reduction potentials⁹ and apart from considerations such as fine-tuning of the molybdenum site and the aforementioned possibility of stabilizing product complexes through hydrogen bonding, there is no suggested mechanistic role for serine 147. While EPR data and EXAFS data together support the structure shown in Figure 3A, the EXAFS data alone cannot a priori distinguish between the structures shown in Figure 3, and we therefore turn to DFT calculations for additional support as to which alternative is the most likely.

DFT Calculations. Calculations were carried out both with and without constraints based on the crystal structure of the enzyme.¹¹ The *P* and *Q* molybdopterin cofactors are relatively large organic moieties held within two substantial clefts in the protein on opposite sides of the molybdenum via a network of hydrogen bonds and van der Waals interactions. Because of this the molybdopterin cofactors are unlikely to move dramatically from their crystallographically observed positions.¹¹ Similarly, serine 147 is located on a short loop bounded by serine 143 and alanine 149 with no obvious secondary structure, so that only subtle flexibility is expected in the positions that this residue can adopt. We therefore chose to constrain the pyran ring of the molybdopterin and the α -C atom of Ser147 at their crystallographically determined coordinates.¹¹ For the purposes of making lengthy calculations more tractable, the molybdopterin was truncated at the pyran ring and terminated by hydrogen coordination. Geometry optimizations of the Mo(V) structures shown in Figure 1 C and Figure 3 were carried out, with selected results summarized in Table 2 and shown in Figures 6 and 7. Unconstrained refinements tended to produce geometries in which the two molybdopterins deviated substantially from their crystallographic positions. This is shown in Figure 6, which compares constrained and unconstrained optimizations for structure 3A, and shows a relative angular motion of the *Q* molybdopterin of about 15°. This

Table 2. Selected Computed DFT Bond-Lengths^a

bond	structure					
	1C	3A	3B	3C	XAS-1	XAS-2
Mo–OH(2)	2.04	1.90	2.42		1.99	2.36
Mo–O(Ser147)	1.99		1.93	2.14		2.00
Mo–S _{average}	2.44	2.37	2.41	2.36	2.35	2.35
RMSD ^b	0.131	0.044	0.061	0.066		

^aInteratomic distances in Å from energy minimized geometry optimized DFT structures. ^bRMSD is the root-mean-square deviation in bond-length with the analogous XAS structure; XAS-1 for five coordinate or XAS-2 for six coordinate structures.

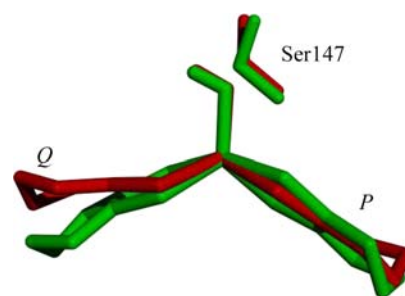


Figure 6. Constrained (green) and unconstrained (red) DFT geometry optimized structures corresponding to Figure 3A.

translates to considerable motion of the more distant parts of the cofactor, which is unlikely and illustrates the desirability of using crystallographic constraints.

When protonated Ser147 is included in structure 3A, the structures 3A and 3B are directly comparable as they have the same charge and atom count. These structures have very similar energies, with 3B having a lower energy by 29 kJ/mol. The high energy of structure 3A is somewhat problematic, but could be relieved by partial relaxation of the constraints discussed above. Thus, the release of all constraints from 3A results in a lowering of energy by 56 kJ/mol, with the Mo adopting a first-coordination shell geometry that is close to square pyramidal. Considering only the first-coordination shell the largest effect of relieving constraints is a change in the improper torsion angle described by the two pairs of sulfur donors (one pair from each of the two molybdopterins) from 20° to 0.5°, with the latter describing nearly square pyramidal geometry (i.e., all four sulfurs are nearly in the same plane). One issue with using rigid crystallographic restraints is that in reality, and unlike the pterin portion of the molybdopterin, the less rigid pyran ring can undergo limited flexure allowing partial rotation of the aforementioned improper torsion angle. Thus, while the use of some sort of constraints or restraints is clearly advisable (e.g., Figure 6), a more extended calculation in which the distant parts of the molybdopterin were rigidly constrained would likely be more realistic. Such calculations would involve many more atoms than currently used (the DMSO reductase Mo site including both molybdopterins amounts to 154 atoms) which would make calculations rather more demanding computationally. Another approach is to use a combination of molecular mechanics and DFT, with the former specifying the protein component and the latter the metal-containing active site.⁴² We propose to investigate both approaches in subsequent work. For the present, we conclude that DFT alone cannot distinguish which of the two structures is more likely. If the EXAFS-derived and DFT-computed bond-lengths are compared then, as expected, the best match is with the five-coordinate structure 3A with a root-mean-square bond-length deviation (RMSD) value of only 0.044 Å; the six-coordinate species 1C and 3B have RMSD values of 0.131 and 0.061 Å, respectively. The structure 3C with bound protonated Ser147 is similar to 3B at 0.066 Å. For structure 3A the largest mismatch is for the Mo–O bond for which the EXAFS derived bond-length is longer by 0.09 Å, which is outside the expected discrepancy of the two techniques, although the discrepancy for the Mo–S bonds is excellent at 0.02 Å, being substantially responsible for the low RMSD.

Comparison with Protein Crystallography. The crystal structure of DMSO reductase is unusual among the

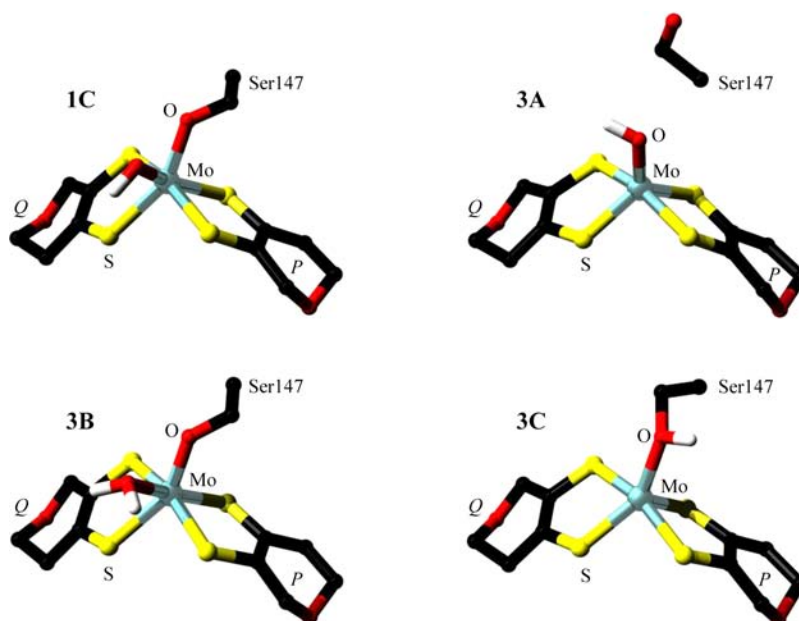


Figure 7. Constrained DFT geometry optimized structures corresponding to Figure 1C and Figure 3A, B, and C. With the exception of groups directly coordinating the molybdenum, hydrogen atoms have been omitted for clarity. The furan ring of the molybdopterin cofactor was included using the constraints discussed in the text.

molybdenum enzymes in that it is thought to represent the enzyme in the fully oxidized Mo(VI) state. Many other molybdenum enzyme crystal structures show evidence of photoreduction of the molybdenum site by the X-ray beam,^{4,43} and it is possible that partial reduction is present, but undetected, with DMSO reductase crystal structures. The highest resolution 1.3 Å DMSO reductase crystal structure shows fractional occupancy of two sites cocrystallized, called site A and site B.¹¹ Site A is attributed to a structure corresponding to an inactive form of the enzyme, has a *cis*-dioxo Mo with one cofactor dithiolene dissociated, and comprises about 60% of the enzyme in the crystal. Site B is thought to correspond to fully active enzyme and resembles Figure 1B; we consider only site B in the following discussion. The crystal structure shows a number of anomalous structural features associated with serine 147.¹¹ The Mo–O–C(Ser147) angle deduced from crystallography is 162° which is much larger than the chemical norm, a search of the Cambridge Structural Database²⁷ yielding a mean value for such a bond of 126°. Also, the (Ser147)O–Mo–S₁₂ angle deduced crystallographically is 61°;¹¹ the smallest such angle in the Cambridge database is 77° with a sterically hindered bidentate ligand,⁴⁴ and the mean value for this coordination was 125°.²⁷ We note in passing that the fractional occupancy of the two chains A and B used in the crystallographic analysis differs from 25% to 40% of B in different places in the protein,¹¹ suggesting that there are more than just the two forms A and B cocrystallizing. The anomalous structural details of serine 147 obtained from crystallographic analysis suggest that there may be some inhomogeneity of this ligand, perhaps because of partial photoreduction and dissociation of the serine, adds weight to the conclusions from our EXAFS analysis.

CONCLUSIONS

The evidence presented here suggests that serine 147 is dissociated from molybdenum in the high-*g* split Mo(V) EPR signal giving species. Based on catalytic turnover experiments⁶

and upon spectroscopic measurements⁷ it has previously been proposed that the species is a bona fide catalytic intermediate. The results presented here indicate that previous structures postulated for this species, and the basis of previous spectroscopic interpretations and calculations, are likely incorrect. In *R. sphaeroides* periplasmic nitrate reductase the well-studied proton-split signal called the “high-*g* signal” has been shown to arise from an inactive “dead-end” form of the enzyme, with no detectible Mo(V) EPR arising from the active form.⁴⁵ The possibility that the DMSO reductase high-*g* split species is a similar dead-end species seems an unlikely one, however, as there is no loss of activity associated with its formation and it accumulates to almost 100% in turnover experiments.⁶ If the high-*g* split were catalytically inactive then the observed turnover would need to be due to a quite small (and undetected) quantity of a very active species. We note that in the reaction mechanism of DMSO reductase as generally understood, the Mo(V) species is generated in the reductive limb of the catalytic sequence, as the oxidized Mo(VI) enzyme receives reducing equivalents on reduction to Mo(IV) and prior to reaction with DMSO. *In vitro*, these reducing equivalents typically come from sodium dithionite, but *in vivo* are thought to be delivered by the pentaheme DorC protein (with reducing equivalents ultimately derived from the quinone pool).⁴⁶ It is generally understood that the Mo(V) state is not generated in the course of the reaction of reduced enzyme with DMSO (or TMAO), which is considered to occur via a normal oxygen atom transfer. Given the alternatives discussed above further work is needed to shed additional light on the nature of the signal-giving species and its role, if any, in catalysis. For example, proton ENDOR might confirm the absence of a second more weakly coupled exchangeable proton (i.e., for prospective Mo–OH₂ coordination) or the absence of hyperfine coupling from the serine 147 alpha proton. Moreover, our DFT calculations could be expanded by using combined molecular mechanics and quantum mechanical methods. The results presented here also suggest a hitherto

unsuspected flexibility of serine 147 in DMSO reductase in that it appears to be able to dissociate from the Mo. Whether or not this has any relevance to the enzyme catalytic cycle remains an open question.

AUTHOR INFORMATION

Corresponding Author

*E-mail: g.george@usask.ca.

Notes

The authors declare no competing financial interest.

ACKNOWLEDGMENTS

We thank Professor Martin L. Kirk for commenting on this manuscript in advance of publication. Work carried out at the University of Saskatchewan was supported by the Natural Sciences and Engineering Research Council of Canada, with other support from a Canada Research Chair (G.N.G.) and the Canadian Institutes of Health Research (CIHR) and the Saskatchewan Health Research Foundation (SHRF). M.J.P. and J.J.H.C. are Fellows in the CIHR Training grant in Health Research Using Synchrotron Techniques (CIHR-THRUST). M.J.P. is a CIHR Postdoctoral Fellow and is also supported by SHRF. Further support was available from PrioNet Canada. Research at the University of California was supported by the National Institutes of Health (ES 012658, R.H.). Portions of this research were carried out at the Stanford Synchrotron Radiation Lightsource, a Directorate of SLAC National Accelerator Laboratory and an Office of Science User Facility operated for the U.S. Department of Energy Office of Science by Stanford University. The SSRL Structural Molecular Biology Program is supported by the DOE Office of Biological and Environmental Research, and by the National Institutes of Health, National Center for Research Resources, Biomedical Technology Program (P41RR001209). This research has been enabled by the use of WestGrid computing resources, which are funded in part by the Canada Foundation for Innovation, Alberta Innovation and Science, BC Advanced Education, and the participating research institutions. WestGrid equipment is provided by IBM, Hewlett-Packard, and SGI.

REFERENCES

- (1) Magalon, A.; Fedor, J. G.; Walburger, A.; Weiner, J. H. *Coord. Chem. Rev.* **2011**, *255*, 1159–1178.
- (2) Hille, R.; Nishino, T.; Bittner, F. *Coord. Chem. Rev.* **2011**, *255*, 1179–1205.
- (3) Williams, R. J. P.; Fraúso da Silva, J. J. R. *Biochem. Biophys. Res. Commun.* **2002**, *292*, 293–299.
- (4) Pushie, M. J.; George, G. N. *Coord. Chem. Rev.* **2011**, *255*, 1055–1084.
- (5) George, G. N.; Johnson Nelson, K.; Harris, H. H.; Doonan, C. J.; Rajagopalan, K. V. *Inorg. Chem.* **2007**, *46*, 3097–3104.
- (6) Cobb, N.; Conrads, T.; Hille, R. *J. Biol. Chem.* **2005**, *280*, 11007–11017.
- (7) Mtei, R. P.; Lyashenko, G.; Stein, B.; Rubie, N.; Hille, R.; Kirk, M. L. *J. Am. Chem. Soc.* **2011**, *133*, 9762–9774.
- (8) George, G. N.; Hilton, J.; Rajagopalan, K. V. *J. Am. Chem. Soc.* **1996**, *118*, 1113–1117.
- (9) George, G. N.; Hilton, J.; Temple, C.; Prince, R. C.; Rajagopalan, K. V. *J. Am. Chem. Soc.* **1999**, *121*, 1256–1266.
- (10) Garton, S. D.; Hilton, J.; Hiroyuki, O.; Crouse, B. R.; Rajagopalan, K. V.; Johnson, M. K. *J. Am. Chem. Soc.* **1997**, *119*, 12906–12916.
- (11) Li, H. K.; Temple, C.; Rajagopalan, K. V.; Schindelin, H. *J. Am. Chem. Soc.* **2000**, *122*, 7673–7680.
- (12) Bennett, B.; Benson, N.; McEwan, A. G.; Bray, R. C. *Eur. J. Biochem.* **1994**, *255*, 321–331.
- (13) Bray, R. C.; Adams, B.; Smith, T. A.; Richards, R. L.; Lowe, D. J.; Bailey, S. *Biochemistry* **2001**, *40*, 9810–9820.
- (14) George, M. J. *J. Synchrotron Radiat.* **2000**, *7*, 283–286.
- (15) Cramer, S. P.; Tench, O.; Yocum, M.; George, G. N. *Nucl. Instr. Meth.* **1988**, *A266*, 586–591.
- (16) <http://ssrl.slac.stanford.edu/exafspak.html>.
- (17) George, G. N.; Garrett, R. M.; Prince, R. C.; Rajagopalan, K. V. *J. Am. Chem. Soc.* **1996**, *118*, 8588–8592.
- (18) Rehr, J. J.; Mustre de Leon, J.; Zabinsky, S. I.; Albers, R. C. *J. Am. Chem. Soc.* **1991**, *113*, 5135–5140.
- (19) Mustre de Leon, J.; Rehr, J. J.; Zabinsky, S. I.; Albers, R. C. *Phys. Rev. B* **1991**, *44*, 4146–4156.
- (20) Delley, B. *J. Chem. Phys.* **1990**, *92*, 508–517.
- (21) Delley, B. *J. Chem. Phys.* **2000**, *113*, 7756–7764.
- (22) Perdew, J. P.; Burke, K.; Ernzerhof, M. *Phys. Rev. Lett.* **1996**, *77*, 3865–3868.
- (23) Perdew, J. P.; Burke, K.; Ernzerhof, M. *Phys. Rev. Lett.* **1997**, *78*, 1396.
- (24) Klamt, A.; Schüürmann, G. *J. Chem. Soc. Perkin. Trans.* **1993**, *2*, 799–805.
- (25) Ferreira, G. C.; Franco, R.; Mangravita, A.; George, G. N. *Biochemistry* **2002**, *41*, 4809–4818.
- (26) Cotelesage, J. J. H.; Pushie, M. J.; Grochulski, P.; Pickering, I. J.; George, G. N. *J. Inorg. Biochem.* **2012**, *115*, 127–137.
- (27) Allen, F. H.; Kennard, O.; Watson, D. G. *Struct. Correl.* **1994**, *1*, 71–110.
- (28) Zhang, L.; Pickering, I. J.; Winge, D. R.; George, G. N. *Chem. Biodivers.* **2008**, *5*, 2042–2049.
- (29) Pushie, M. J.; Zhang, L.; Pickering, I. J.; George, G. N. *Biochim. Biophys. Acta* **2012**, *1817*, 938–947.
- (30) George, G. N. *J. Biol. Inorg. Chem.* **1997**, *2*, 790–796.
- (31) George, G. N.; Garrett, R. M.; Prince, R. C.; Rajagopalan, K. V. *Inorg. Chem.* **2004**, *43*, 8456–8460.
- (32) Qiu, J. A.; Wilson, H. L.; Pushie, M. J.; Kisker, C.; George, G. N.; Rajagopalan, K. V. *Biochemistry* **2010**, *49*, 3989–4000.
- (33) Wang, J.-J.; Tessier, C.; Holm, R. H. *Inorg. Chem.* **2006**, *45*, 2979–2988.
- (34) Lim, B. S.; Holm, R. H. *J. Am. Chem. Soc.* **2001**, *123*, 1920–1930.
- (35) Bertero, M. G.; Rothery, R. A.; Palak, M.; Hou, C.; Lim, D.; Blasco, F.; Weiner, J.; Strynadka, N. C. J. *Nat. Struct. Biol.* **2003**, *10*, 681–687.
- (36) Finnegan, M. G.; Hilton, J.; Rajagopalan, K. V.; Johnson, M. K. *Inorg. Chem.* **1993**, *32*, 2616–2617.
- (37) Hernandez-Marin, E.; Seth, M.; Ziegler, T. *Inorg. Chem.* **2010**, *49*, 1566–1576.
- (38) Jormakka, M.; Richardson, D.; Byrne, B.; Iwata, S. *Structure* **2004**, *12*, 95–104.
- (39) Bray, R. C.; Adams, B.; Smith, A. T.; Bennett, B.; Bailey, S. *Biochemistry* **2000**, *39*, 11258–11269.
- (40) Zhang, L.; Johnson Nelson, K.; Rajagopalan, K. V.; George, G. N. *Inorg. Chem.* **2008**, *47*, 1074–1078.
- (41) Webster, C. E.; Hall, M. B. *J. Am. Chem. Soc.* **2001**, *123*, 5820–5821.
- (42) Hong, G.; Ivnitski, D. M.; Johnson, G. R.; Atanassov, P.; Pachter, R. *J. Am. Chem. Soc.* **2011**, *133*, 4802–4809.
- (43) George, G. N.; Pickering, I. J.; Kisker, C. *Inorg. Chem.* **1999**, *38*, 2539–2540.
- (44) Chaves, S.; Gil, M.; Canário, S.; Jelic, R.; João Romão, M.; Trincão, J.; Herdtweck, E.; Sousa, J.; Diniz, C.; Fresco, P.; Santos, A. J. *Chem. Soc., Dalton Trans.* **2008**, 1773–1782.
- (45) Fourmond, V.; Burlat, B.; Dementin, S.; Arnoux, P.; Sabaty, M.; Boiry, S.; Guigliarelli, B.; Bertrand, P.; Pignol, D.; Léger, C. *J. Phys. Chem. B* **2008**, *112*, 15478–15486.
- (46) Shaw, A. L.; Hochkoeppler, A.; Bonora, P.; Zannoni, D.; Hanson, G. R.; McEwan, A. G. *J. Biol. Chem.* **1999**, *274*, 9911–9914.